國立臺灣大學工學院應用力學研究所

碩士論文

Graduate Institute of Applied Mechanics
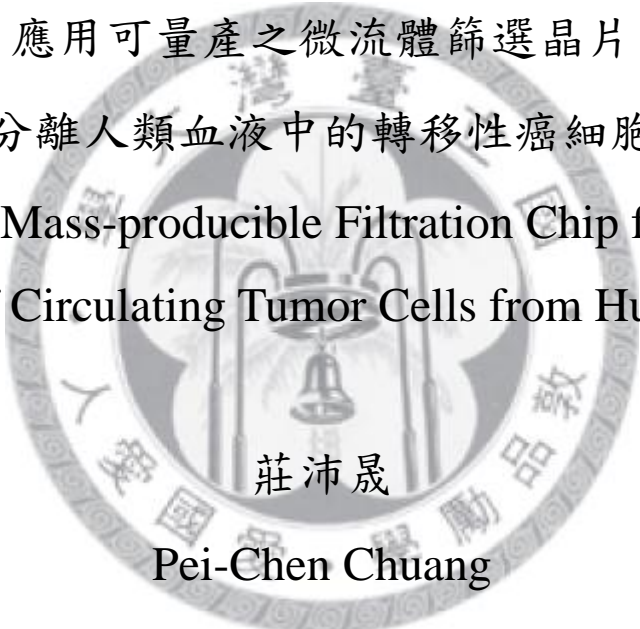
College of Engineering

National Taiwan University

Master Thesis

應用可量產之微流體篩選晶片

分離人類血液中的轉移性癌細胞

A Mass-producible Filtration Chip for

Isolation of Circulating Tumor Cells from Human Blood

莊沛晟

Pei-Chen Chuang

指導教授：胡文聰 博士

Advisor: Andrew M. Wo, Ph.D.

中華民國 101 年 7 月

July 2012

誌謝

中文摘要

　　循環癌細胞 (circulating tumor cells, CTCs) 檢測是一可期待且對病人較少傷害癌症轉移檢測方法。臨床中癌症造成的死亡有九成是來自於癌細胞的轉移，其轉移路徑通常經由進入血管後轉移至腦、骨髓、肺臟、肝臟或其他器官。然而目前循環癌細胞檢測仍未被常規性使用於疾病管理，其中一個原因來自於稀少細胞的汲取困難。本工作及透過一內含以尺寸為篩選標準的微過濾結構之微流晶片從血液中汲取循環癌細胞，其製造方法為精密塑膠射出成形的壓克力製微結構熱壓接合到以電腦數值控制銑床製的壓克力儲存槽。廣範圍之癌症細胞株 (K562, MCF7, PC3 與 Colo205) 被微結構抓取後以螢光染色並以螢光顯微技術計數。結果顯示此晶片之穩定與易用性，以上述細胞株加入一毫升血液 (稀釋為十五毫升) 模擬病人檢體中的循環癌細胞抓取，其回收率達到七至八成。故此微流晶片應擁有讓循環癌細胞檢測成為更可用之癌症管理工具之潛力。

關鍵字：尺寸、稀少細胞、細胞分離、細胞抓取、低價、壓克力、射出成形、量產、循環癌細胞、癌症檢測

ABSTRACT

The detection of circulating tumor cells (CTCs) is a promising harmless in vitro diagnosis of metastasis. Cancer metastasis leads to roughly 90% of deaths of cancer patients. However, CTC detection has not been routinely used for disease management, where one reason for this is the difficulty associated with enrichment of these extremely rare cells. This work presents a microdevice to enrich CTCs from peripheral blood by a size-limiting microfilter structure. This PMMA structure is microinjection-mold and bonded onto a CNC-milled reservoir. Cells from a wide range of cancer cell lines (K562, MCF7, PC3 and Colo205) are captured on the structure, immunohistochemically stained and enumerated with fluorescent microscopy. Results show the chip is robust and ease to use. The recovery yield of cells spiked into 1mL of whole blood (diluted to 15mL) attained 70% to 80%. This microdevice should have potential to enable CTC-detection a more viable in cancer management.

Keywords: size-based; rare cell; cell separation; cell isolation; low cost; PMMA; injection molding; mass-production; Circulating tumor cells; CTCs

CONTENTS

LIST OF FIGURES

LIST OF TABLES

Chapter 1   Introduction

World Health Organization (WHO) indicated cancer as the leading cause of death worldwide for decades. The data, published by WHO in February 2012, showed 7.6 million deaths from cancer in 2008, around 13% of all death, and a promise of escalation estimate that in 2030, cancer would have caused 13.1 million deaths. Roughly 90% of cancer death is due to metastasis.

One known feature of cancer is the rapid growth of abnormal cells which can invade other parts of the body through the bloodstream. Circulating tumor cells (CTCs) are the invading tumor cells in the circulating system, while metastases are the tumor migration processes.[1,2] Cancer-caused deaths were mainly due to the late diagnosis when metastasis has occurred. Metastasis was often diagnosed only when the tumors are big enough for detection with screening technologies or when symptoms clue in to the change, and by then the prognoses are statically unfavorable.[3]

To improve the monitoring of cancer clinical courses, it is essential to have an early detection method for metastasis. Quantities of CTCs have been shown to relate to patients' survival probabilities and disease progressions.[4-8] Enumeration and analysis of CTCs are harmless in vitro cancer monitoring process in late stage cancer patients. However, CTCs are vulnerable and extremely rare compared with hematologic cells, about one CTC to a billion of hematologic cells. Therefore, isolating CTCs from whole blood is a challenge.[9]

Several devices have been published to isolate CTCs from peripheral blood. Generally, conventional cell-isolation techniques are mainly based on immune-separation (using magnetic beads or affinity), density difference (applying special medium integrated with centrifugation) and morphology difference (size and deformability) of target cells. For

example, an immune-separation platform, CellSearch, is a commercial product approved by Food and Drug Administration. The specific marker Epithelial Cell Adhesion Molecule (EpCAM/CD326) of tumor cells was applied to separate CTCs by conjugating magnetic beads coated with EpCAM-specific antibodies.[10-12] Another immune-separation device, herringbone-chip, is the second-generation CTC-chip[13-15] with higher throughput and efficiency, applies passive mixing of blood cells through generation of micro-vortices by the herringbone-like anti-EpCAM coated microstructure to increase the interaction between CTCs and the chip surface.[16] Other methods for CTC-separation without immunoassay included density-based and size-based methods. Among density-based methods, applications of Ficoll-paque or Oncoquick buffer integrated with centrifugation procedures have been established not only for mononuclear cells but also for CTCs-separation.[12,17-22]

Additionally, there are several size-based methods which use the stiffness and size difference between CTCs and hematic cells to isolate target cells from whole blood. A PDMS chip coated with polyurethane-methacrylate with serpentine channels lined with optimized tall rectangular apertures was used for CTCs-filtration.[23] Microfabricated membrane filters with large quantities of pores for letting hematic cells pass through and catch the larger target cells. For example, ISET (Isolation by Size of Epithelial Tumor Cell) was a polycarbonate Track-Etch-type membrane with randomly-positioned pores.[24-27] Another membrane-based filter with regular arrayed pores was fabricated by microlithography processes, which was able to do the nuclei analysis after cell-isolation.[28-31] Besides, there were many PDMS-based devices separate rare cells from peripheral blood by different ways.[32-34]

Although there have been many CTC-detection approaches done to date, CTC-detection has still not generalized as routine health checkups in most of hospitals

worldwide. Part of obstacles may come from the high cost, high processing threshold of operators and the difficulties of device mass-production. The purpose of this study was to develop a size-based CTC-isolation device which is uncomplicated to operate and made of inexpensive material – PMMA – through conventional mass-production methods – injection molding and CNC milling process. The approaches of this research provide a potential device that can be applied in routine health checkups.

Chapter 2 Experimental

2.1 Device design

We designed a slim and thin aperture as the filter unit. As Figure 1(a) shown, a 9µm high opening structure was formed with a first level microstructure (30µm) as the side-support and a second level microstructure (21µm) as the base. While cells sample flowed through the opening, large cells would most likely retain along the edge and/or lodged into the inner wall. This feature was designed not only to trap multiple cells but also to relieve localized pressure due to spaces between closely packed cells. The openings formed by bonding neighboring supports (100µm(W) × 50µm(L)) with ceiling (Figure 1(b)) are lined along the filter-structured wall. To achieve high throughput, the filter-structured wall is distributed as serpentine around the inlet opening (area: 1cm by 1cm) of the device (Figure 1(c)). In this device, there are over 3000 openings according to the pattern density. A layout with many opening structures safeguarded the captured cells from the huge fluid drag. Once an opening occludes, rest of the openings still allowed the carrier fluid to flow through.[23]

To increase the detection rate of target cells, the slim transverse openings is installed to ensure that target cells will not overlap vertically but form a monolayer after filtration. Therefore, it promises an easier way to accurately show results by just detecting with similar focal length in the selected areas along the filter-structured wall.

With the device design, samples entered the chip perpendicular to its plane and proceed parallel to surface, similar to that in stagnation point flow in 3 dimensions. Without using features of microchannel, the unique flow structure enhanced the sample processing. Furthermore, the planer filter-structure design would potentially simplify the photolithography fabrication of the master for replica molding. Fabrication using a

high-strength mechanical material would be robust and allow for easy handling.
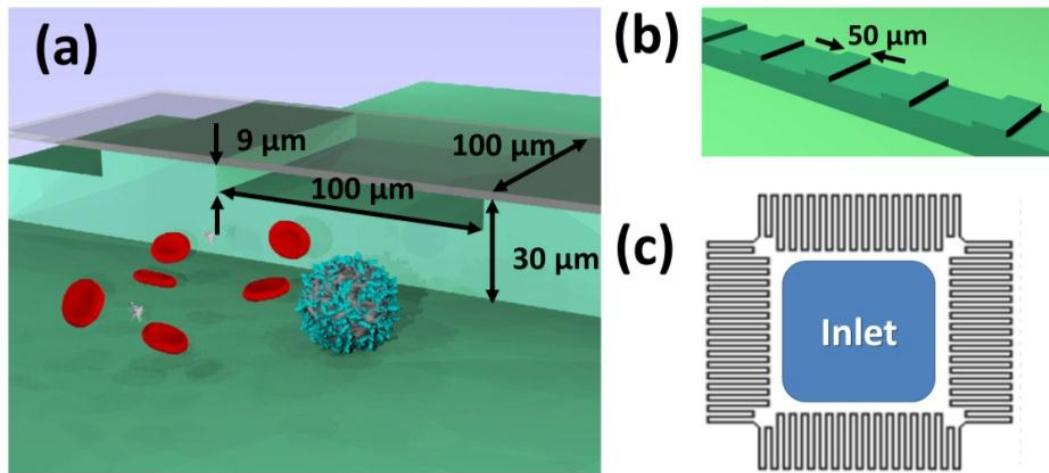
Figure 1 Device design. *(a) Illustration of the filtration mechanism. Blood cells in a 30μm-high chamber between the ceiling cover. The opening structure: 9μm× 100μm× 100μm. (b) Design of a linear array of the opening structure. (c) Serpentine linear array of the filters surrounding the inlet, 1cm by 1cm.*

2.2 Device Fabrication

The filtration chip was fabricated using two approaches: the inlet opening by CNC machining and the filter structure by micro injection molding. For large scale tests, devices made by injection molding should be effective for validation. The standard mass production process and rapid pilot run procedure make it feasible for a quick trial of the fabrication instead of lab-wise hand-made devices. The expense is acceptable comparing with clean-room fabrication devices in a laboratory. As for the material, Poly-methylmethacrylate (PMMA) and polycarbonate (PC) are both the common thermoplastic materials with high transparency for mass production. We chose PMMA because it is an economical alternative to PC if extreme strength is not necessary. Additionally, PMMA does not contain the potentially harmful bisphenol-A subunits found in PC raised further concerns regarding exposure of fetuses, infants, and young children.

Multiple chip patterns were micro-injection molded on a 12cm PMMA disc by the CD/DVD manufactory (RITEK Inc., Taiwan) and were cut to needed dimension, see Figure 2(a). The single filter structure and the inlet opening were shown by Figure 2(b) and 2(c). For each pilot run, there are at least 3,000 pieces of disc produced and 15,000 filter structures fabricated. The cost of each micro filter, for a two-level structure, was less than $0.30 USD.
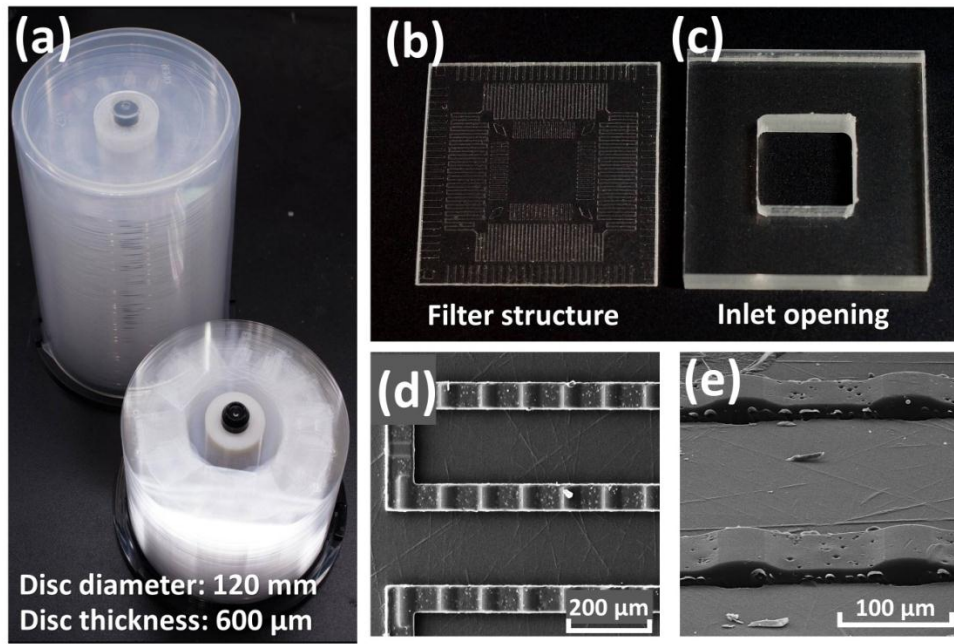
Figure 2 The fabricated chip spares. *(a) CD/DVD- like PMMA discs. (b) Single filter structure (2.5cm × 2.5cm). (c) The inlet opening (opening: 1 cm × 1 cm) for sample loading. (d)(e) SEM image of the micro filter.*

2.3   Device assembly

Figure 3(a) shows the filtration chip. The device was composed of the inlet opening and the filter structure. The two parts are assembled using plasma-enhanced thermal bonding.[35] A custom made pressure chamber was used to control the variation of the aperture sizes. In the process, oxygen plasma pretreatment and the temperature control were necessary. The temperature was set under $70^{\circ}C$ in order to make the filter-structure moderately deformed. Actually, the expected sizes of the aperture applied for CTC isolation was 5~8µm. Recall the previous filter design, we believed the captured cancer cells should deform while physically against the micro structures and encounter with fluid drag. So we design the aperture with a 9µm height in advance, leaving 1~4µm as sacrifice during the bonding process. With this method, it provided a

flexibility of fine-tuning aperture high while there was only one size of filter structure fabricated.
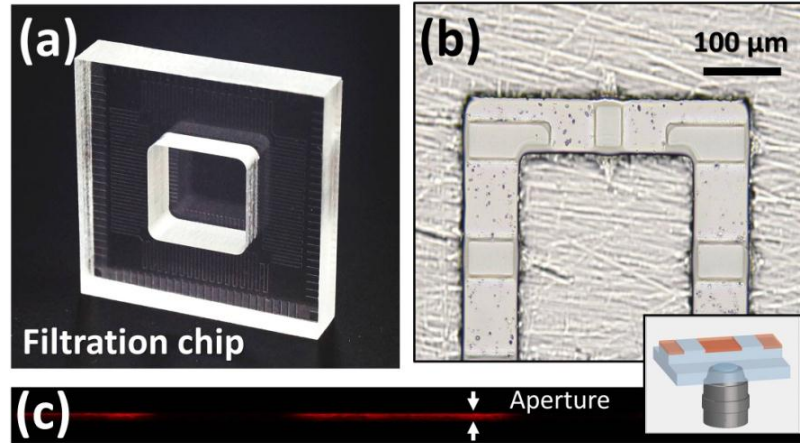
Figure 3 The assembled filtration chip. *(a) The filtration chip was composed of two parts: inlet opening and the filter structure. (b) The bright-field image of the filter structure. (c) 3D reconstructed cross-sectional image of the apertures.*

Figure 3(b) shows the bright field image of the microstructures. The image confirmed the bonding of supporting structure with the top ceiling. To verify the aperture sizes and the effects of plasma-thermal bonding, the filtration chip were examined by a florescence confocal microscopy. The chip was fulfilled with a fluorescent dye (Rhodamine B, Sigma-Aldrich, Inc.) and then the images of the apertures at different focal-planes along the z-axis were taken. As shown in Figure 3(c), the reconstructed image, based on an image stack of 0.8μm vertical step size showed the vertical cross section of the aperture. With the image, an examined device with an aperture of 6 ± 0.8μm was assembled under these conditions: oxygen-plasma treatment (40sccm, 100W, 1min), thermal-bonding (70 ℃, uniform pressure of 8 kgw/cm^2 in 20 min).

2.4   Experimental setup

An apparatus for chip-tubeless setup was designed to ensure stable filtration of blood sample with high cell viability under a suction system. The custom made chamber connected with a pressure gauge and a vacuum pump, as shown in Figure 4(a)-(b). The filtration chip was clamped between with a center-opening lid and the chamber. The gastight environment formed an only way, from outside to chamber, through the apertures of the filtration chip. We termed the pressure difference between the ways through apertures as:

$$\Delta P = P_{inlet} - P_{chamber}$$

Once the constant ΔP was given, the sample in the inlet would be derived to flow through the micro filters and the waste would be remained in the chamber, as illustrated by Figure 4(c). In the suction chamber, there was no tubing needed to connected with the filtration chip. Therefore, there was no pressure variation occurred due to pressure transferred discontinuously if once there were waste transported in tubing.
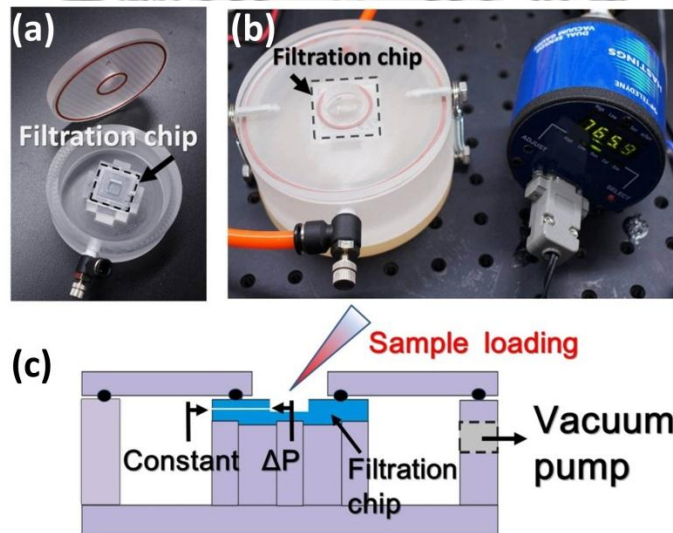
Figure 4 The experimental setup. *(a) The filtration chip and the suction chamber. (b) The filtration chip was clamped within the suction chamber. The pressure was indicated by a pressure gauge. (c) Sketch of the suction chamber with the filtration chip.*

2.5   Experimental procedure

In the experimental procedure, the constant ΔP was set to a pressure value controlled by a regulator. A volume of 1ml running buffer was first introduced to the chip for rinsing. After that, the prepared cell sample was loaded into chip for filtration. The processing time was depended on the sample volume and dilution condition. After filtration, 3ml of running buffer was used to rinse the chip to remove the residual cells or other particles. If necessary, repeated the previous procedure with dye staining and buffer washing. Finally, the filtration-chip was removed to the fluorescence microscope for image detection.

2.6   Cell culture and preparation

Human breast adenocarcinoma cell line (MCF-7), erythroleukemic cell line (K562), colorectal adenocarcinoma cell line (Colo205), and the prostate adenocarcinoma cell line (PC3) were used to verify the chips for isolation different CTCs from hematic cells. K562, PC3 and Colo205 were cultured in RPMI medium 1640 (Gibco/Invitrogen) and MCF-7 was cultured in DMEM/F-12 medium (Gibco/Invitrogen). Both medium were added with 10% fetal bovine serum, 1% penicillin-streptomycin and 1.2~2g/L sodium bicarbonate. All the cell lines were incubated in tissue culture dishes at the environment of 5% CO_2 and 37°C.

Prior to introduce into the filtration chip, cells were detached from the culture dish, treated in 0.05% trypsin-ethylenedinitriletetraacetic acid (trypsin-EDTA) in a 37 ℃ incubator for 5 min, and then resuspended in medium achieving around 10^6 cells/mL. Cell counts were estimated by using hemocytometer.

Selected cell line samples, staining and fixation, were according to different tests to process. For the chip characterization (not patient samples), pre-staining was applied. With concentration of ~100 cells/µL (MCF-7, PC3, K562 or Colo205) was first labeled with anti-EpCAM-PE by adding 10µl anti-EpCAM-PE and then incubated for 20 minutes at room temperature. As fixation, 1mL of 2% formaldehyde was added to cell pellet, via centrifugal process and then mixed by pipetting. After 20 min incubation in room temperature, the formaldehyde solution was then substitute by PBS via centrifugal process.

After treatments, the sample was diluted with its culture medium to a concentration of ~10 cells/µL. Cell counts were measured by spreading 10µL cell sample on a glass slide and then with microscope. Finally cell counts were determined as the average of three repeated quantifications, which the coefficient of variation (CV) should be controlled below 10%.
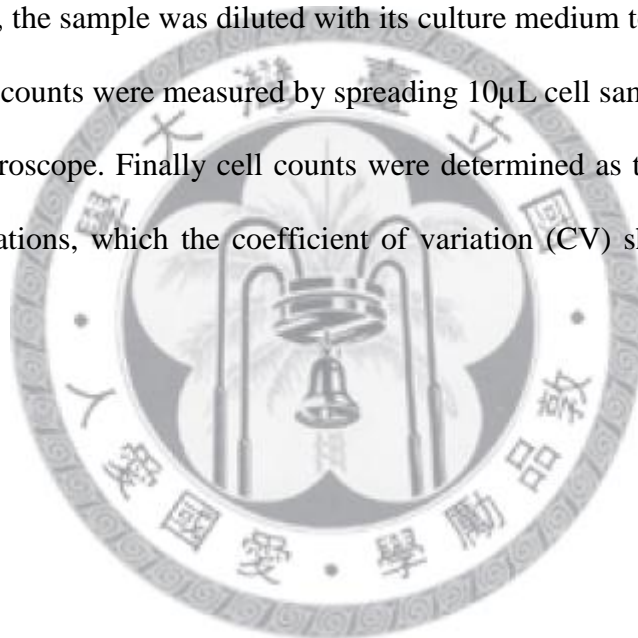
2.7   Cell size measurement

To measure the diameter distribution of cell population, each of the cultured cell lines was suspended in PBS stained with Calcein AM. With a concentration of 103 cells/mL, 10μl of the stained cells was sprayed on a glass slide and then wait for 20 min for cells sedimentation.

For a rapid characterization, a microscope with a digital camera (Nikon D5100, 1.6 M pixels, connected with a 1.5X conversing ring) was used for image capture. The captured image resulted in a high resolution, which is around 1.5µm/pixel at 2X object lens and 0.6µm/pixel at 5X. The images were analyzed using the software of Image J.

2.8   Blood dilution and preparation

Simulation of human blood for cancer patients was prepared from the whole human blood of healthy donators. The blood samples were stored at 4 °C until the experiments performed. Each sample was collected using BD Vacutainer tube with sodium heparin. To ensure the blood samples fresh, the experiments should be processed within 24 hours.

For mimicking cancer patient sample, the blood samples were diluted with PBS to a volume ration of 15X and spiked with the prepared cancer cells. In general, the known quantities of cultured tumor cells, ~100 to 250 cells, were spiked in each blood sample.

2.9   Cell viability assay and culture on chip

Cultured tumor cells mixed with blood form healthy donors were filtered through the device, washed with PBS, and loaded with culture medium. Then replace the device to a petri dish cultured for 2days in an incubator at 5% CO_2 and 37℃. On the 2nd day, the device was washed with PBS. Acetomethoxy derivate of calcein (calcein AM, C3100MP, Invitrogen) was added to the device for 30 min. Calcein AM can transport through the cellular membrane into cells then be hydrolyzed by an intracellular enzyme resulting in strong green fluorescence. As dead cells lack this enzyme, only live cells are marked. Fluorescent images were taken via the CCD camera (Leica 360) using a fluorescence microscope (IX-71, Olympus).

2.10   Immunofluorescent (IF) analysis

For visually distinguishing cancer cell lines or CTCs from hematic cells with fluorescence microscope, the on-chip staining (post-staining) process was applied. The captured cells were sequentially fixed with Inside Fix, permeabilized with Inside Perm, intracellular-stained with anti-Cytokeratin-FITC (expressed green signal), surface-stained with EpCAM-PE (expressed red signal) and nuclear-stained with Hoechst 33342 (expressed blue signal). All the processes involved repeatedly keeping liquid with reagents on-chip for cell fixing, permeabilization, incubation and final washing with PBS. Each staining/labeling required 20 minutes incubation at room temperature. Finally, the IF images were took using a 10X fluorescent microscope (Olympus IX71) fit with a CCD camera (Leica DFC360FX).

Chapter 3   Results and Discussion

3.1   Capture efficiency and cell size

Since CTCs are extremely rare in blood, it is important to maximize its capture efficiency. We have characterized the capture efficiency with different samples using our filtration device.

Polystyrene beads (10μm) were used for preliminary test. With very low concentration in the phosphate buffered saline (PBS) (3 beads/ml), the device had 100% capture efficiency (n=3) due to the less deformability of the beads.

Table 1 shows the capture efficiency of the device using three different cancer cell lines. For live tumor cell of MCF-7 (sample A in Table 1), device with 6±0.8μm aperture had 87.3±1.5% efficiency under a constant negative pressure of 0.1psi. The major cause for capture efficiency lose was believed to be cell deformability that allow the small cells to pass through. Therefore, we have characterized the size of cell population and found the percentage of the small cells (≤ 8μm) was around 16% and large cells (≥ 9μm) around 84%, see Figure 5. The percentage of large cells (~84%) was close to the capture efficiency. This implied that the filtration device has a pass window for the cell sizes around 8μm under a negative pressure of 0.1psi. The results highly depended on the size distribution of cell samples. To confirm the assumption, we tested another MCF-7 sample. Results (sample B in Table 1) showd the device had 94±2.1% capture efficiency. As expected, the cut off line of the filtration device performance was still around 8μm, since the percentage of the large cells in this sample was around 92% and close to the capture efficiency. The results indicated the filtration device made by micro-injection molding is robust.

Testing other cell lines, Colo205 and PC-3, those tests showed the capture efficiency

differs with different cell lines/populations. Nevertheless, the pass window of cell size with other cell lines was still around 8μm. It is worth to note that the yield of MCF-7 (sample A) was higher (2.9% +) than the percentage of large cells; and the same correlation occurred in the same cell line of sample B (1.6% higher +), as well as Colo205. However, in PC-3 cell line, the yield was lower (3.3% -) which may come from different rigidity of cell compared with other cell lines.

Tested sample	Size	Loaded cell/bead Number	Capture efficiency
Beads	10μm	3	100%
MCF-7 (sample A)	0~30μm > 9μm **(84.4%)**	185±8	**87.3±10.1%**
MCF-7 (sample B)	0~30μm > 9μm **(92.4%)**	92±6	**94.0±10.2%**
Colo205	0~30 um >9μm **(65.8%)**	58±2	**74.5±14.9%**
PC-3	0~30um >9μm **(83.5%)**	123±6	**80.2±4.9%**

Table 1　Capture efficiency of micro-beads and three different cell lines in PBS tested at 0.1psi negative pressure.
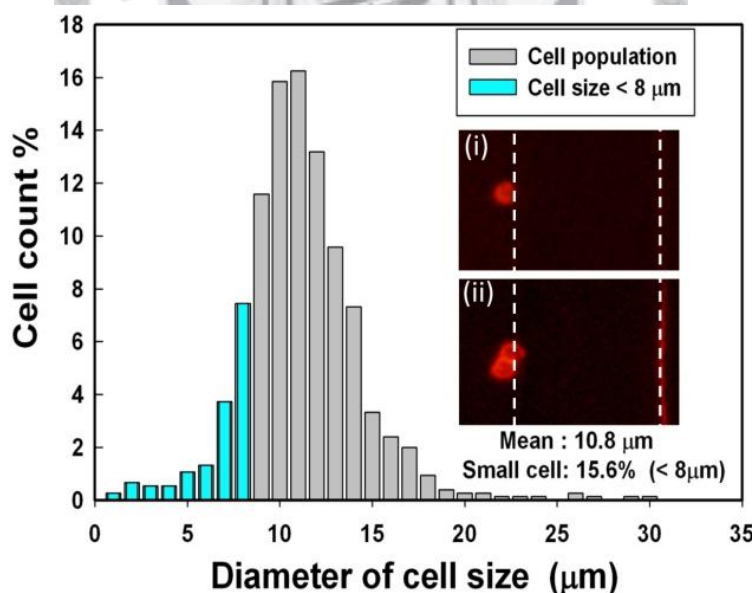

Figure 5　Size distribution of MCF-7 (sample A) cell line. The inset figures show one and two cells (with PE-anti-EpCAM) captured on the aperture of the filtration chip, and their sizes are larger than 9μm.

3.2   Effects of ΔP and cell condition on yield

To optimize the workable pressure in our experimental setup, we have characterized the pressure of the filtration device with cell membrane fixation. Filtration using high ΔP may have high efficiency but also can cause cells lysis.

Figure 6 shows the yields according to different cell conditions (fixed/unfixed) and pressure. With fixed MCF-7 cells, the yield was 103.5±8.7% at 0.1 psi, and 93.6±8.0% at 0.7 psi. With unfixed MCF-7, the results showed dramatic drop of yield from 88.2±10.4% at 0.1psi down to 13.0±11.7% at 0.3psi. The results showed that rigidity of cells plays an important role in size-based filtration. It is worth to noting that rapid decrease of yield was occurred between 0.1psi and 0.3psi. This may indicate most unfixed cells damaged or deformed then went through the apertures exceed 0.3psi.
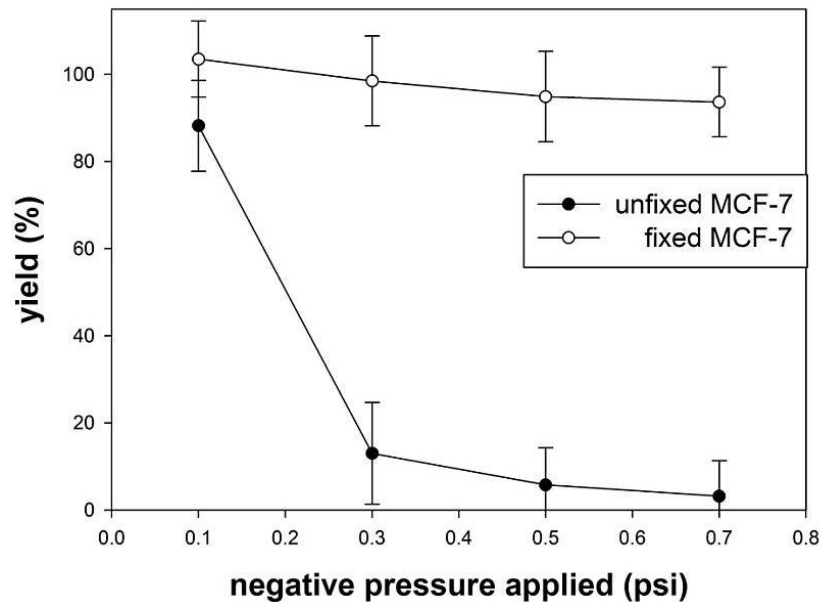
***Figure 6 Effects of ΔP and the rigidity of cells on yield in filtration processing.** Rigidity of cells highly affected the yield of cells, especially as ΔP exceeded 0.3 psi. Results of each experimental data based on three replicas.*

3.3   Viability studies of captured cells

For viability test, PC-3 prostate cancer cell line was introduced to the filtration device. After 48 hours, captured cells were stained on-chip with Calcein AM. Figure 7 shows the results that cells are viable and even proliferating, which enable further cell culture and other analysis of rare cells.
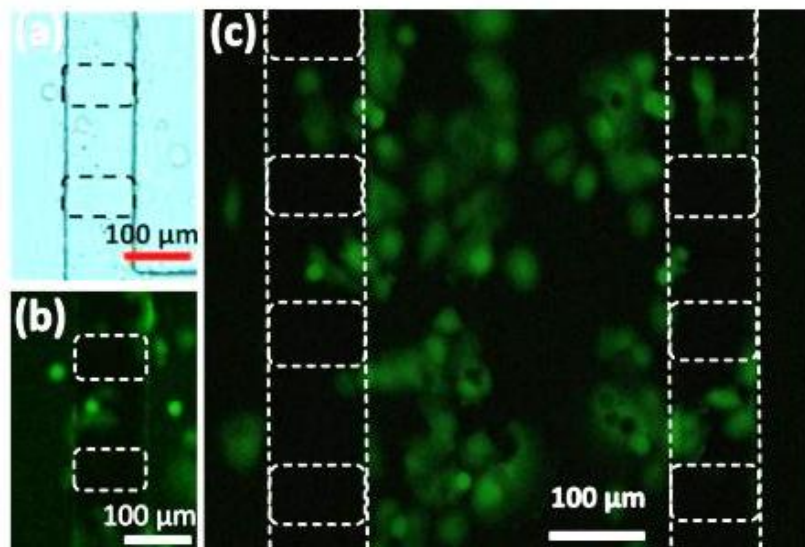
Figure 7 Viability of captured cells after 48 hours incubation. (a) Captured cells in bright filed and (b) in green fluorescence. (c) Fluorescent image (stained with Calcein AM) shows the captured cells are alive and proliferating around the aperture.

3.4   Effects of dilution ratio

Blood dilution can prevent cell aggregation which may cause most cells clogged and decrease the performance. In sample pretreatment, whole blood was diluted to ratio of 15x (sample 1) and 30x (sample 2) with buffer relatively, and then the targeted cells (MCF-7 pre-stained with EpCAM-PE) were spiked into samples. Table 2 shows the device with diluted sample 2 had high processing rate which indicated the sample of high dilution ratio is likely to have low viscosity and less cellular aggregation. Concerning the total cell number (whole blood volume) processing rate, device handle with sample 1 was about 1.5 times greater than that of sample 2. The yields were 80 % in sample 1 and 89 % in sample 2.

Figure 8 shows the processing rate of the filtration device with two different diluted samples. Below 1mL of filtered whole blood, the processing rates of both samples were linear which demonstrated the stability of our filtration device. Additionally, the device stocked before 1mL whole blood filtered while using under the dilution ratio under 5X. Therefore, the limitation of whole blood volume was set as 1mL for one single device and the dilution ratio to 15x for following experiments.

| Condition	Sample 1 (15x)	Sample 2 (30x)
Cell line	Unfixed MCF-7	Unfixed MCF-7
Whole blood	1.0 mL	0.5 mL
Diluted blood	15.0 mL	15.0 mL
ΔP applied	0.1 psi	0.1 psi
Results		
Processing time	~ 70 min	~ 54 min
Blood handling efficiency	0.86 mL/hr	0.56 mL/hr
Yield of MCF-7	80 %	89 %

Table 2   Results of spiked cells in blood with different dilution ratio
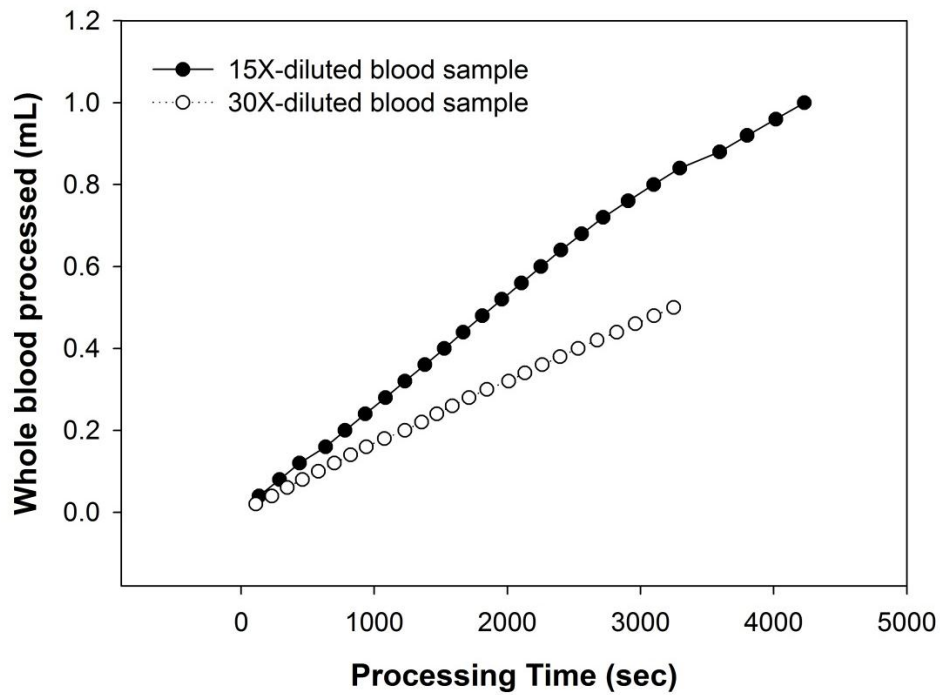
Figure 8 Processing rate with two diluted blood samples. Results show the processing rate of each experiment seems to be linear which indicates the filtration device with the suction system is reliable.

3.5   Yield of Tumor cell lines spiked in healthy blood

We mimicked different kinds of cancer patient samples by spiking ~102 Colo205, PC3, MCF7 (labeled with EpCAM-PE) and K562 (labeled with hoechst-DAPI) with 1mL of human blood from healthy donators and then diluted with 14mL PBS before processed by our device. It took about 1 to 1.5 hours to complete the filtration. Figure 9 shows the result that the yield of each sample was 69.3±24.3% (Colo205), 78.0±14.9% (PC3), 80.0±10 % (MCF-7) and 70.3±13.9% (K562) respectively. The yields fell at around 70-80% in different types of cancer cell line samples. The results showed that the yields do not depend on EpCAM expression of each cell line, which Colo205 and MCF7 are high EpCAM expression, PC3 is medium EpCAM expression and K562 is EpCAM-negative.
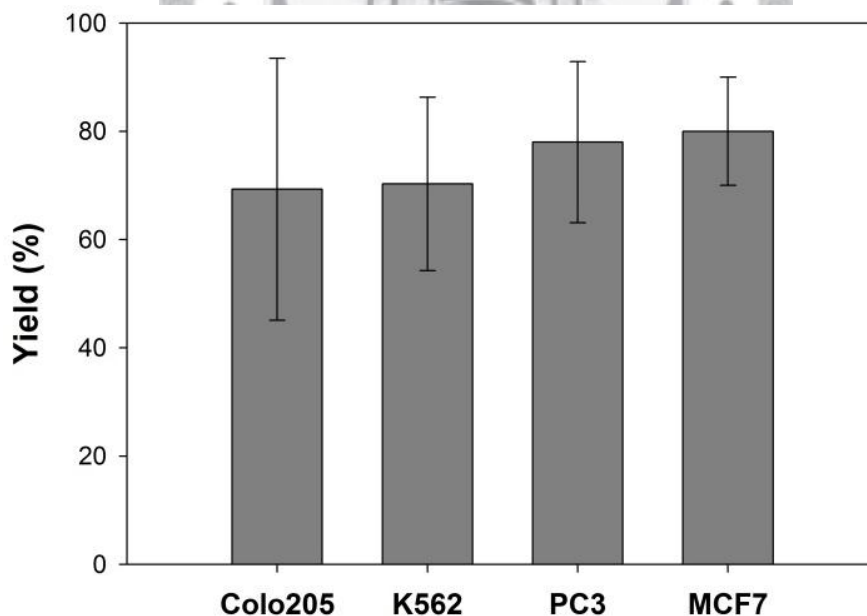
Figure 9 Yields of mimicking cancer patient samples. *Cancer cells of Colo205, PC3 and MCF7 were spiked in human blood from healthy donators. The represented data was measured with three replicas*

Chapter 4   Conclusion

The presented mass-producible filtration chips have demonstrated high capture efficiency. With 100% capture efficiency on 10μm beads. For unfixed tumor cell line MCF-7, the device has 87.3±1.5% capture efficiency under a constant negative pressure of 0.1psi. Other cell lines tests showed the capture efficiency would change if use different cell lines/populations. Due to the injection-molding production, the performance of the low-cost device is robust.

The recovery rate of live MCF-7 cells spiked in diluted blood is 80~89%, of Colo205, PC3 and K562 are 70% to 80%. The filtration chip could handle 15mL diluted blood (1:15) in 1~1.5 hour. For cell viability test, PC-3 prostate cancer cell line was testes to show after 48 hours filtration, and stained on-chip with Calcein AM are viable and even proliferating, which enable further cell culture and other analysis of rare cells. The system setup for chip tubeless was show the stability of performance and high cell viability. With the aspects of low cost, tubeless, high capture efficiency and viable capture makes this device enables further cell analysis and other experiments of these value cells.

Reference

(1)   P. S. Steeg Nat Med 2006, 12 (8), 895-904.

(2)   S. Mocellin, U. Keilholz, C. R. Rossi, D. Nitti Trends Mol Med 2006, 12 (3), 130-139.

(3)   J. Kaiser Science 2010, 327 (5969), 1072-1074.

(4)   M. Cristofanilli Semin Oncol 2006, 33 (3), S9-S14.

(5)   S. Mocellin, D. Hoon, A. Ambrosi, D. Nitti, C. R. Rossi Clin Cancer Res 2006, 12 (15), 4605-4613.

(6)   G. Wiedswang, B. Naume Nat Clin Pract Oncol 2007, 4 (3), 154-155.

(7)   S. Riethdorf, H. Wikman, K. Pantel Int J Cancer 2008, 123 (9), 1991-2006.

(8)   J. S. de Bono, H. I. Scher, R. B. Montgomery Clin Cancer Res 2009, 15 (4), 1506-1506.

(9)   J. den Toonder Lab Chip 2011, 11 (3), 375-377.

(10) M. Naoe, Y. Ogawa, J. Morita, K. Omori, K. Takeshita, T. Shichijyo, T. Okumura, A. Igarashi, A. Yanaihara, S. Iwamoto, T. Fukagai, A. Miyazaki, H. Yoshida Cancer 2007, 109 (7), 1439-1445.

(11) S. Riethdorf, H. Fritsche, V. Muller, T. Rau, C. Schindibeck, B. Rack, W. Janni, C. Coith, K. Beck, F. Janicke, S. Jackson, T. Gornet, M. Cristofanilli, K. Pantel Clin Cancer Res 2007, 13 (3), 920-928.

(12) J. Kraan, S. Sleijfer, M. H. Strijbos, M. Ignatiadis, D. Peeters, J. Y. Pierga, F. Farace, S. Riethdorf, T. Fehm, L. Zorzino, A. G. J. Tibbe, M. Maestro, R. Gisbert-Criado, G. Denton, J. S. de Bono, C. Dive, J. A. Foekens, J. W. Gratama Cytom Part B-Clin Cy 2011, 80B (2), 112-118.

(13) R. J. Lee, S. L. Stott, S. Nagrath, L. E. Ulkus, D. M. Dahl, M. R. Smith, M. Toner,

S. Maheswaran, D. A. Haber J Clin Oncol 2009, 27 (15),

(14) L. V. Sequist, S. Nagrath, M. Toner, D. A. Haber, T. J. Lynch J Thorac Oncol 2009, 4 (3), 281-283.

(15) S. Nagrath, L. V. Sequist, S. Maheswaran, D. W. Bell, D. Irimia, L. Ulkus, M. R. Smith, E. L. Kwak, S. Digumarthy, A. Muzikansky, P. Ryan, U. J. Balis, R. G. Tompkins, D. A. Haber, M. Toner Nature 2007, 450 (7173), 1235-U10.

(16) S. L. Stott, C. H. Hsu, D. I. Tsukrov, M. Yu, D. T. Miyamoto, B. A. Waltman, S. M. Rothenberg, A. M. Shah, M. E. Smas, G. K. Korir, F. P. Floyd, A. J. Gilman, J. B. Lord, D. Winokur, S. Springer, D. Irimia, S. Nagrath, L. V. Sequist, R. J. Lee, K. J. Isselbacher, S. Maheswaran, D. A. Haber, M. Toner P Natl Acad Sci USA 2010, 107 (43), 18392-18397.

(17) E. E. Lagoudianakis, A. Kataki, A. Manouras, N. Memos, A. Papadima, A. Derventzi, G. Zografos, S. Papadopoulos, V. Katergiannakis, M. M. Konstadoulakis J Surg Res 2009, 155 (2), 183-190.

(18) V. Muller, N. Stahmann, S. Riethdorf, T. Rau, T. Zabel, A. Goetz, F. Janicke, K. Pantel Clin Cancer Res 2005, 11 (10), 3678-3685.

(19) R. Gertler, R. Rosenberg, K. Fuehrer, M. Dahm, H. Nekarda, J. R. Siewert Recent Res Cancer 2003, 162 149-155.

(20) R. Rosenberg, R. Gertler, J. Friederichs, K. Fuehrer, M. Dahm, R. Phelps, S. Thorban, H. Nekarda, J. R. Siewert Cytometry 2002, 49 (4), 150-158.

(21) E. Andreopoulou, L. Y. Yang, K. M. Rangel, J. M. Reuben, L. Hsu, S. Krishnamurthy, V. Valero, H. A. Fritsche, M. Cristofanilli Int J Cancer 2012, 130 (7), 1590-1597.

(22) V. Melnikova, Y. Zhang, M. Pace, M. Garza, S. Sukumaran, S. Zhao, J. Woo, D. Davis Ejc Suppl 2010, 8 (7), 196-196.

(23) J. S. Kuo, Y. X. Zhao, P. G. Schiro, L. Y. Ng, D. S. W. Lim, J. P. Shelby, D. T. Chiu Lab Chip 2010, 10 (7), 837-842.

(24) G. Vona, A. Sabile, M. Louha, V. Sitruk, S. Romana, K. Schutze, F. Capron, D. Franco, M. Pazzagli, M. Vekemans, B. Lacour, C. Brechot, P. Paterlini-Brechot Am J Pathol 2000, 156 (1), 57-63.

(25) V. De Giorgi, D. Massi, M. Grazzini, P. Pinzani, T. Lotti J Am Acad Dermatol 2011, 64 (2), Ab9-Ab9.

(26) I. Desitter, B. S. Guerrouahen, N. Benali-Furet, J. Wechsler, P. A. Janne, Y. A. Kuang, M. Yanagita, L. L. Wang, J. A. Berkowitz, R. J. Distel, Y. E. Cayre Anticancer Res 2011, 31 (2), 427-441.

(27) V. Hofman, C. Bonnetaud, M. I. Ilie, P. Vielh, J. M. Vignaud, J. F. Flejou, S. Lantuejoul, E. Piaton, N. Mourad, C. Butori, E. Selva, M. Poudenx, S. Sibon, S. Kelhef, N. Venissac, J. P. Jais, J. Mouroux, T. J. Molina, P. Hofman Clin Cancer Res 2011, 17 (4), 827-835.

(28) S. Zheng, H. Lin, J. Q. Liu, M. Balic, R. Datar, R. J. Cote, Y. C. Tai J Chromatogr A 2007, 1162 (2), 154-161.

(29) H. K. Lin, S. Y. Zheng, A. J. Williams, M. Balic, S. Groshen, H. I. Scher, M. Fleisher, W. Stadler, R. H. Datar, Y. C. Tai, R. J. Cote Clin Cancer Res 2010, 16 (20), 5011-5018.

(30) T. Xu, B. Lu, Y. C. Tai, A. Goldkorn Cancer Res 2010, 70 (16), 6420-6426.

(31) S. Y. Zheng, H. K. Lin, B. Lu, A. Williams, R. Datar, R. J. Cote, Y. C. Tai Biomed Microdevices 2011, 13 (1), 203-213.

(32) A. Chatterjee, S. S. Kuntaegowdanahalli, I. Papautsky Proc Spie 2011, 7929

(33) S. J. Tan, L. Yobas, G. Y. H. Lee, C. N. Ong, C. T. Lim Biomed Microdevices 2009, 11 (4), 883-892.

(34) S. M. McFaul, B. K. Lin, H. Ma Lab Chip 2012, 12 (13), 2369-2376.

(35) C. S. Tan, A. Fan, K. N. Chen, R. Reif Appl Phys Lett 2003, 82 (16), 2649-2651.

Appendix A   Design concepts of apertures on the micro-filter

This section is talking about the reasons we designed the micro-filter. First, we chose rectangle as the shape of apertures because of the simplicity in multi-layer photolithography fabrication of the mold for injection-molding. For simpler detection, the short transverse of the rectangular aperture should be the height to ensure the target cells will not be overlapping after filtration.

In addition, various dimension and arrangement of the apertures generate different pressure fields encountered by a cell in a filtration environment. It was necessary to analyze how the design of apertures affects the cells because cell membrane has its tolerance to neighboring pressure. There were several studies about cell membrane damage associated with mechanical trauma. For example, micropipette experiments on artificial phospholipids, similar to cell membrane, demonstrated that membrane damage happened when membrane tension increased over a critical level, i.e. membrane area extension outpace 3% (Evans et al. 1979). Cell lysis occured at the tension as low as 3 mN/m (Kwok and Evans 1981). Therefore, to prevent the probability of cell rupture and lysis during filtration process, the aperture was needed to be designed for lowering the pressure on the cell membrane.

A brief analysis (Daniel T. Chiu, 2010) of hydrodynamic pressure conveyed encountered by a spherical particle by the carrier fluid in various filtration environments is in sections below. Three simplified filtration conditions experienced by a spherical particle will be discussed respectively: (1) carrier fluid flows past a spherical particle; (2) a spherical particle captured by a single aperture; and (3) a spherical particle occluding an aperture in the presence of multiple parallel apertures.

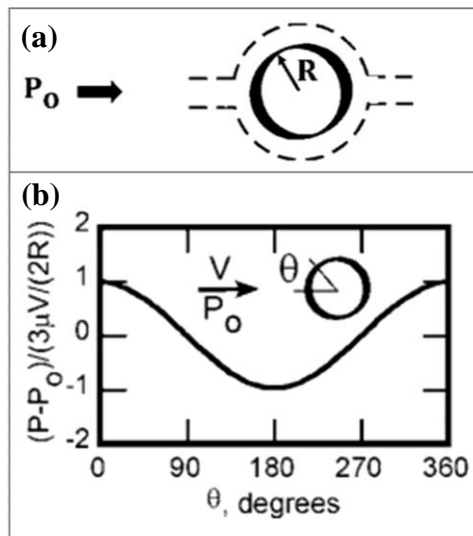**Condition 1: Carrier fluid flows past a free spherical particle.**

In the condition of the carrier fluid flow past a free spherical particle (Figure 10 (a)), the theoretical local pressure distribution (P), received from the fluid, around the particle is different from the angle θ (Figure 10 (b)). To showed the local pressure distribution around the particle in equation,

$$P = P_0 + \frac{3}{2}\frac{\mu V}{R}\cos\theta$$

where Po is the upstream pressure (for convenience, we assumed the downstream pressure to be 0), m is the viscosity of the carrier fluid, R is the radius of the particle, and V is the relative velocity of the fluid. The maximum pressure is at θ = 0°; the minimum pressure is at θ = 180° on the particle surface; so that the maximum pressure difference (ΔP_{max}) is:

$$\Delta P_{max} = 3\frac{\mu V}{R}$$

In filtration processing, the local pressure distribution around the particle and the maximum pressure difference were mechanical force probable to made the cell damaged. In the equation (1) and (2), the parameter we could tune, while filtering, were V and P_0. The optimization of V and P_0 will be discussed in section 2.3.
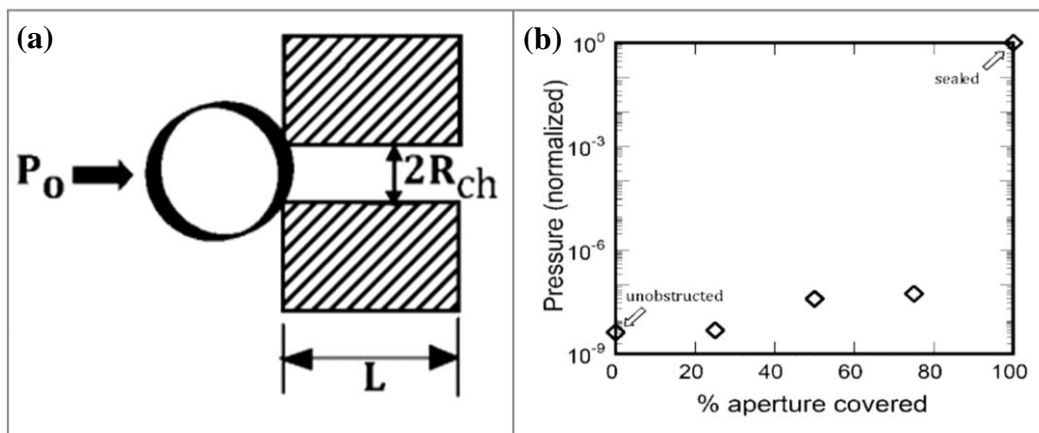
Figure 10   Analysis of the pressure experienced by the spherical particle in the condition of carrier fluid flows bypass

(a) Carrier fluid flows past a free spherical particle and (b) pressure distribution on the surface (Daniel T. Chiu, 2010)
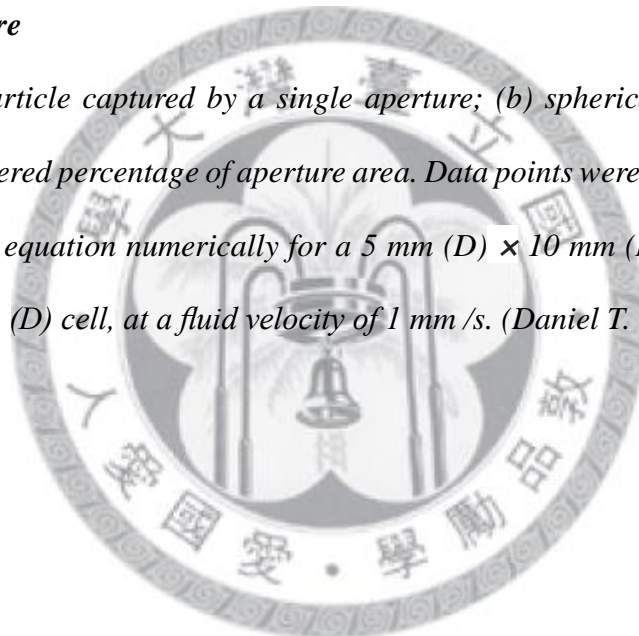
Condition 2: a spherical particle captured by a single aperture

While a spherical particle captured by a single aperture (Figure 11 (a)) in the filtration processing, the pressure that carrier fluid imparting to the spherical particle strongly depended on the covered ratio of aperture area. Figure 11 錯誤! 找不到參照來源。 (b) illustrates the normalized spherical particle pressure versus various covered percentage of aperture area. The spherical particle pressure while the aperture totally blocked were at about 10^7 and 10^9 times as large as the spherical particle pressure while ~75% aperture covered and aperture unobstructed. Obviously, to ensure the flow bypass, i.e. to ensure the aperture not to be sealed, was important to prevent the cells encountering the large pressure which was probable to cause cell damage in filtration processing.

Figure 11   *Analysis of the pressure experienced by the captured spherical particle*

by a single aperture

(a) A spherical particle captured by a single aperture; (b) spherical particle pressure versus various covered percentage of aperture area. Data points were obtained by solving the Navier–Stokes equation numerically for a 5 mm (D) × 10 mm (L) channel partially blocked by a 5 mm (D) cell, at a fluid velocity of 1 mm /s. (Daniel T. Chiu, 2010)

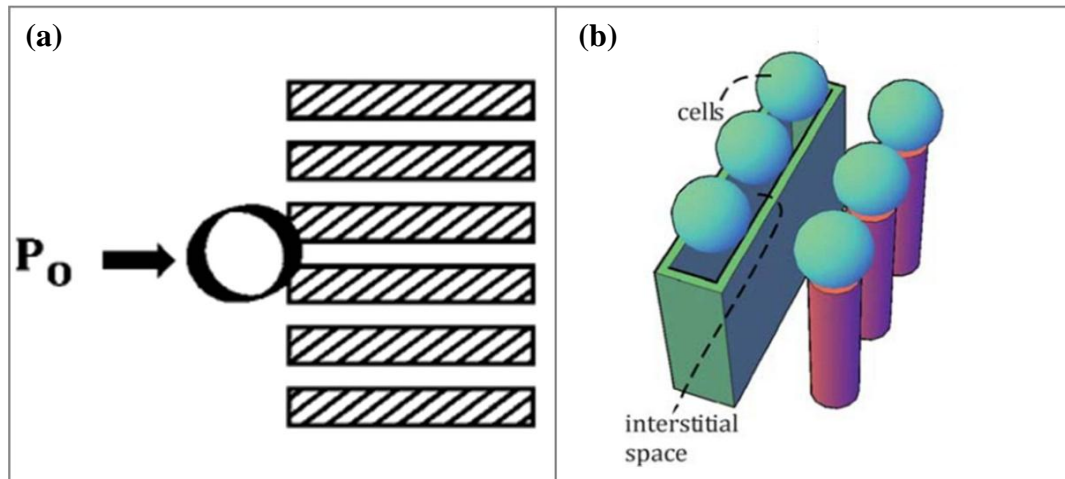**Condition 3: A spherical particle occluding an aperture in the presence of multiple parallel apertures**

In this case (Figure 12 (a)), one of the parallel apertures was blocked by a single particle. Meanwhile, the other apertures were still unobstructed and allowed the carrier fluid to flow bypass. For one unblocked parallel channel, the pressure difference between the inlet and outlet of the channel ($\Delta P_{channel}$) came from viscous dissipation which was related to viscosity of the carrier fluid (μ), hydrodynamic diameter of the channel ($D_{channel}$) the length of the channel (L) and the velocity of the carrier fluid (V). The viscous dissipation of one unblocked parallel channel could be calculated with the equation:

$$\Delta P_{channel} = \frac{32\mu VL}{D_{channel}^2}$$

For n parallel channels, the pressure difference between the inlet and outlet of the channels became

$$\Delta P_{n-channel} = \frac{32\mu VL}{nD_{channel}^2}$$

That is, the pressure difference experienced by the captured spherical particle was equal to the pressure drop of the channel, which could be lowered to $\frac{1}{n}$ times with n parallel channels.

*Figure 12   Multiple parallel apertures and the shape design*

(a) A spherical particle occluding an aperture in the presence of multiple parallel apertures; (b) The rectangular aperture had interstitial space for flow bypass even though the captured cells connecting to each other closely but the independent single apertures had not.

In conclusion, the aperture design was not only about the apertures with key size for separating the cells by size but also the arrangement and dimension of the apertures which could prevent the cell damage while filtering. After analyzing from the condition one to three, first of all, the aperture dimension was decided to be 100µm (W) × 8µm (H). The width of the rectangular aperture (100µm) could prevent the aperture dead blocked. Even though there were more than one cells captured by the same aperture, there still had interstitial space for flowing bypass (Figure 12 (b)). The second, the apertures were parallel, not independent to each other. The design safeguarded the captured cells from the huge incensement once the channel occluded because rest of the channels still allowed the carrier fluid to flow bypass. Finally, there were over 2000 apertures lined on the serpentine filtration part of the chip. The quantity of apertures was not only for promoting flow rate (larger total area of aperture section) in the same giving pressure but also for reducing $\Delta P_{channel}$ (see eqn. (4), larger the n).

Appendix B Thermal bonding chamber system

For reaching the thermal bonding environment (normal stress and temperature), a thermal bonding system was designed. The thermal bonding system was a system built up with two aluminum blocks with caves which could form a chamber between them while they were combined (Figure 13 (a)). The bottom one with PMMA dummy (Figure 13 (b)) which could be changed to feat the shape of the spares. And the top one was attached with a slice of membrane (Figure 13 (c)), which could endure the pressure from high-pressure nitrogen. While high-pressure nitrogen applied to the top chamber, the membrane (with O-ring between two blocks to prevent leakage) transferred normal stress to the spares. For keeping the bonding temperature, the hotplate was set under the bonding chamber. With stable pressure, temperature and flat surfaces on the spares to be bonded, the spares could be assembled.
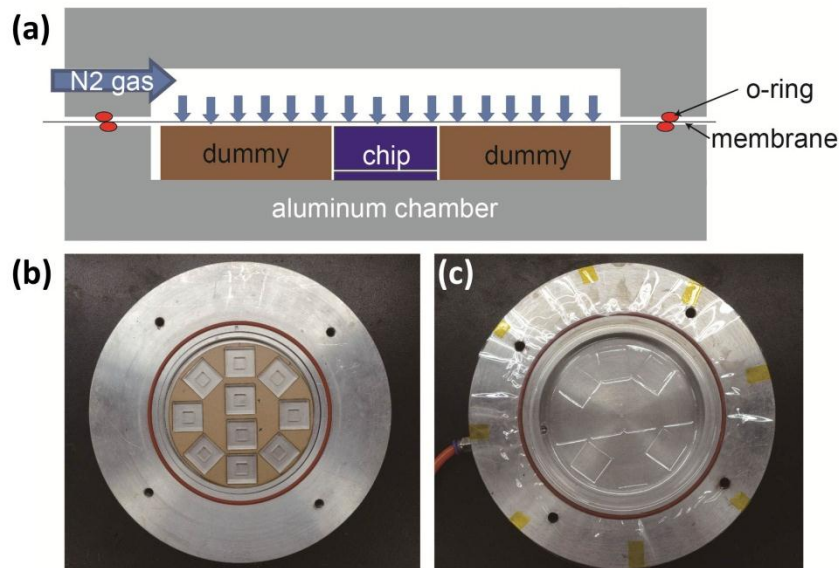
Figure 13   Thermal bonding chamber system (a) a perspective cartoon drawing of the bonding chamber applied with nitrogen (b) the bottom block of the bonding chamber with PMMA dummy and chip spares in it (c) the top block of the bonding chamber with a tube connected with nitrogen bottlenkllm